Economic Performance of Membrane Distillation Configurations in Optimal Solar Thermal Desalination Systems

Desalination

Revised: 17 September 2019

Vasiliki Karanikola,[b, †] Sarah E. Moore,[a, †] Akshay Deshmukh,[b,c] Robert G. Arnold,[a] Menachem Elimelech,[b,c*] and A. Eduardo Sáez [a *]

[a]*Department of Chemical and Environmental Engineering, University of Arizona, Tucson, AZ 85721, USA*

[b]*Department of Chemical and Environmental Engineering, Yale University, New Haven, CT 06520, USA*

[c]*Nanosystems Engineering Research Center for Nanotechnology-Enabled Water Treatment (NEWT), Yale University, New Haven, CT 06520, USA*

[†]V.K. and S.E.M. contributed equally to this work.
* Corresponding Authors:
Eduardo Saez: phone: +1 (520) 621-5369; e-mail: esaez@email.arizona.edu
Menachem Elimelech: phone: +1 (203) 432-2789; e-mail: menachem.elimelech@yale.edu

Abstract

In this study we provide a comprehensive evaluation of the economic performance and viability of solar membrane distillation (MD). To achieve this goal, process models based on mass and energy balances were used to find the minimum cost of water in MD systems. Three MD configurations: direct contact, sweeping gas, and vacuum MD, were compared in terms of economic cost and energy requirements in optimized, solar-driven desalination systems constrained to produce 10 m^3 d^{-1} of distillate from 3.5% or 15% salinity water. Simulation results were used to calculate the water production cost as a function of 13 decision variables, including equipment size and operational variables. Non-linear optimization was performed using the particle swarm algorithm to minimize water production costs and identify optimal values for all decision variables. Results indicate that vacuum MD outperforms alternative MD configurations both economically and energetically, desalting water at a cost of less than $15 per cubic meter of product water (both initial salt levels). The highest fraction of total cost for all configurations at each salinity level was attributed to the solar thermal collectors—approximately 25% of the total present value cost. Storing energy in any form was economically unfavorable; the optimization scheme selected the smallest battery and hot water tank size allowed. Direct contact MD consumed significantly more energy (primarily thermal) than other MD forms, leading to higher system economic costs as well.

TOC Art

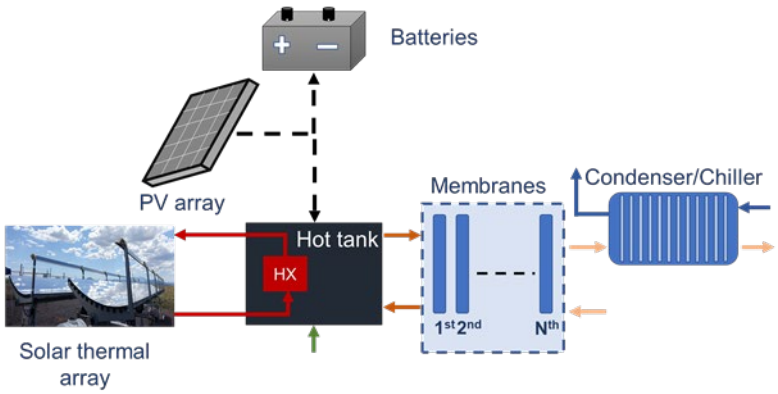

1. Introduction

Water scarcity is among the most pressing challenges facing humanity, impacting over 2.7 billion people worldwide [1-3]. Remote regions lacking public utility infrastructure are among the areas most heavily affected by water scarcity. They are often inhabited by developing communities and marginalized populations, for which the consequences of water shortage are far more reaching. Many such regions experience economic water scarcity, where there is access to non-potable water sources such as saline and hypersaline ground waters, but regional governance lacks the funds to develop these supplies [4, 5].

Off-grid desalination is a feasible alternative for mitigating water scarcity in these areas. More specifically, membrane distillation (MD) is a thermal desalination process that can treat high-salinity waters when conventional pressure-driven desalination processes are limited by high pressure requirements [6, 7]. Thermal desalination processes are energy intensive; however, MD can sometimes satisfy energy demands using low grade or waste thermal energy [7-10]. Solar-driven MD is a promising solution for off-grid desalination in the context of the energy-water nexus as it can reduce the overall energy demand by using low grade heat [11, 12].

There are four main MD configurations that differ by the mechanism of water vapor collection from the permeate stream [13, 14]: direct contact MD (DCMD), sweeping gas MD (SGMD), vacuum MD (VMD), and air gap MD (AGMD). All use heat to transfer liquid water across a hydrophobic membrane as a vapor. DCMD and AGMD condense the water vapor within the same membrane module; DCMD condenses the vapor into a chilled distillate permeate stream, while AGMD uses a cold surface near the membrane surface. SGMD and VMD, on the other hand, require an external condenser. SGMD uses an air stream to sweep the water vapor to the condenser, whereas in VMD water vapor is transferred from the membrane module to the condenser under vacuum.

Each configuration has advantages and disadvantages associated with energy efficiency, water vapor flux, methods of condensation, and thermal energy recovery (Table 1) [15-17]. While DCMD is the simplest configuration, heat transfer through the membrane leads via conduction generally to low thermal efficiency [13]. The introduction of an air gap (AGMD) decreases conductive heat losses and improves thermal efficiency but introduces an additional resistance to mass transfer and reduces water flux [18]. SGMD provides a compromise between DCMD and

AGMD; the sweeping gas improves mass transfer over AGMD, while maintaining low conductive heat loss and high thermal efficiency. However, SGMD increases electrical energy requirements for gas transport, and the presence of the sweep gas requires an external condenser to produce liquid water [19]. Additionally, recovering the heat of vaporization of water is more difficult in SGMD and VMD than in DCMD and AGMD. Both AGMD and DCMD can recover thermal energy within the membrane module—AGMD via the cooling plate adjacent to the permeate stream and DCMD via the continuously chilled distillate [20]. Finally, VMD yields high water flux with virtually no heat loss due to conduction [21]. However, like SGMD, VMD requires external condenser and makes thermal energy recovery difficult. Additionally, VMD requires a vacuum pump, increasing the risk of membrane wetting due to lower pressure on the permeate side of the membrane. While the advantages and disadvantages are well known, quantitative comparisons of these configurations are scarce [22, 23], and particularly for off-grid solar MD desalination systems.

TABLE 1

Several previous studies have modelled off-grid desalination systems to estimate their cost or energy efficiency [24-32]. In these, important factors were sometimes ignored, leading to variation in unit water cost by as much as four orders of magnitude [11, 33]. Most studies did not use comprehensive process models and neglected important considerations such as unsteady operation due to diurnal or seasonal variation in solar irradiance [29]. Some calculated and optimized energy efficiency, while assuming that the most energetically efficient system is also cost-optimal [26, 27, 31, 32]. Most importantly, previous studies generally considered only one MD configuration with one energy source and cited cost estimates for other system configurations [24, 27, 31, 32]. However, as cost estimates are conditional, a cost comparison among alternate MD systems is only valid if calculated under the same set of circumstances. One study concluded that DCMD was the lowest cost option using solar thermal energy, while AGMD was the most expensive [29]. When the cost of thermal energy was neglected (i.e., based on use of waste thermal energy), VMD was the most cost effective, while AGMD remained the most expensive. Additional work to compare optimized MD systems on the same basis is justified.

Herein we compare the economic performances of three membrane distillation configurations — DCMD, SGMD, and VMD — in optimized, solar-driven desalination systems under transient

operational conditions. Simulations led to water production costs as a function of key decision variables including the size of individual system components and operational parameters. Non-linear optimization using a particle swarm algorithm identified decision variable values that minimize either water production costs or energy use. Economically and energetically optimal systems were compared to determine the best membrane distillation configuration for point-of-use desalination. Cost distributions of the three MD configurations are exposed through cost and energy analyses on system components.

2. Modeling and optimization methods

2.1. Solar Membrane Distillation Systems.

The process flow diagrams for the three systems examined (DCMD, SGMD, and VMD) are illustrated in Figs. 1-3. Each system operates in a semi-batch mode by feeding saline water of an initial salinity to a hot water tank (cooling water in). During daily operation, the salinity of the water in the tank increases modestly as the concentrated brine re-enters the tank, where it is mixes with less saline feed water. Mass balance results indicate that over a month of semi-continuous operation, increased salinity in the feed tank does not significantly impact process performance (by lowering the brine-side vapor pressure in the membrane module). Equipment sizes and operational conditions are system decision variables (indicated in italics in the following process descriptions). Stream numbers correspond to those in the figures.

In the DCMD system (Fig. 1), the saline feed enters the hot water tank of volume V_{HT} (Stream 13). Solar thermal energy is collected using an array of solar thermal collectors of total area A_{th} and transferred to hot water tank via a glycol loop (Stream 1). The heated glycol circulates through a heat exchanger in the hot water tank before returning to the thermal collectors (Stream 2). The heated saline feed passes through an array of N_{mod} flat-sheet membrane modules arranged in parallel at a total flow rate of Q_{hw} (Stream 3). Distilled water is continuously chilled to 25 $^{\circ}$C and passed through the membrane modules counter to the direction of the heated saline feed at a flow rate Q_{pw} (Stream 9). Rejected brine is returned to the hot water tank to conserve energy (Stream 4), and makeup saline feed water is added continuously to fill up the hot tank (Stream 13). Permeate exits the membrane module in the chilled water stream (Stream 5), where it is cooled by a heat exchanger of area A_{hx}. The cooled distilled (product) water that exits the heat exchanger (Stream 6) is divided into two streams: (i) the distilled water stream used to meet the daily water

production requirement (Stream 7) and (ii) the remaining distilled water (Stream 8), which is chilled to 25 ºC before being recirculated to the membrane array (Stream 9). Thermal energy is recovered from the hot distilled water by circulating feed (cooling) water (Stream 10) through the heat exchanger at a flow rate of Q_{cw} (Stream 11). The heated cooling water that exits the heat exchanger (Stream 12) is divided into two streams: Stream 13 is used to maintain the volume of water in the hot water tank, and the remaining cooling water (Stream 14) is discarded. Electricity is provided (Line 15) to the three pumps and chiller by a photovoltaic array of area A_{pv} (Lines 17-21). A battery bank sized to operate with a maximum depth of discharge (*DOD*) provides electrical energy when sunlight is insufficient (Line 16). Note that the chiller was added to maintain ambient temperature at the entrance of the membrane module (distillate side) to support direct comparison to SGMD in which air enters at 25 ºC.

FIGURE 1

In the SGMD system (Fig. 2), saline feed enters the hot water tank of volume V_{HT} (Stream 13). Solar thermal energy is collected using an array of solar thermal collectors of area A_{th} and transferred to a glycol loop (Stream 1). The glycol is circulated to a heat exchanger in a hot water tank and returned to the thermal collectors (Stream 2). Heated saline feed is circulated to an array of N_{mod} flat-sheet membrane modules arranged in parallel at a flow rate of Q_{hw} (Stream 3). Permeate diffuses across the membrane into ambient air that passes through the module at a total flow rate Q_{air} (Stream 4). Rejected brine is returned to the hot water tank to conserve thermal energy (Stream 5), and makeup saline feed water continuously replaces permeate to fill up the hot tank (Stream 13). Moist air exits the membrane module (Stream 6) and is sent to a condenser with exchange area A_{cond}. Condensed water and cooled air exit the condenser (Stream 7) and are divided into two streams: (i) the condensed product water (Stream 8), and (ii) the cooled air with any uncondensed water vapor, which is discarded (Stream 9). Thermal energy is recovered from the hot water vapor by circulating cooling (saline feed) water (Stream 10) through the condenser at a flow rate of Q_{cw} (Stream 11). The heated cooling water exiting the condenser (Stream 12) is divided into Stream 13, which is used to maintain the volume of water in the hot water tank, and the remaining cooling water (Stream 14) is discarded. Electricity is provided (Line 15) to the three pumps and blower by a photovoltaic array of area A_{pv} (Lines 17–21). A battery bank with a depth of discharge (*DOD*) provides electrical power when sunlight is insufficient (Line 16).

169 FIGURE 2

170 In the VMD system (Fig. 3), saline feed enters the hot water tank of volume V_{HT} (Stream 12).
171 Solar thermal energy is collected using an array of solar thermal collectors of area A_{th} and
172 transferred to a glycol loop (Stream 1). The glycol is circulated to a heat exchanger in the hot
173 water tank and returned to the thermal collectors (Stream 2). Heated saline feed is circulated to an
174 array of N_{mod} flat-sheet membrane modules arranged in parallel at a flow rate of Q_{hw} (Stream 3).
175 Permeate is drawn across the membrane under vacuum at a pressure of P_v. Rejected brine is
176 returned to the hot water tank to conserve heat (Stream 4), and makeup saline feed water enters
177 the tank to fill up the hot tank (Stream 12). Water vapor exits the membrane module (Stream 5)
178 and is sent to a condenser of area A_{cond}. Condensed water exits the condenser under vacuum
179 (Stream 6) and is stored in a vacuum tank pending discharge as product (Stream 8). The gas in the
180 head space is removed at a flow rate equal to the volume displaced by the condensed permeate to
181 maintain the vacuum pressure (Stream 7). Thermal energy is recovered from the hot water vapor
182 by circulating the cooling (saline feed) water (Stream 9) through the condenser at a flow rate of
183 Q_{cw} (Stream 10). The heated cooling water exiting the condenser (Stream 11) is divided into
184 Stream 12, which is used to maintain the volume of water in the hot water tank, and the remaining
185 cooling water (Stream 13) which is discarded. Electricity is provided (Line 14) to the three pumps
186 and vacuum by a photovoltaic array of area A_{pv} (Lines 16–20). A battery bank with a depth of
187 discharge *DOD* again provides electric power when sunlight is insufficient (Line 15).

188 FIGURE 3

189 **2.2. Process Modeling.**

190 A schematic describing the process model and optimization procedure is provided (Fig. 4).
191 The three MD systems were modeled and optimized in MATLAB using methods previously
192 described [7, 33-35]. Here designs were constrained to produce 10 m^3 d^{-1} of purified water.
193 Necessary input parameters included site-specific data (altitude, latitude, longitude, and ambient
194 temperature for the period of operation simulated) and thermodynamic constants (Supplementary
195 material). The process model simulates operation throughout a single day. Necessary input
196 parameters such as solar irradiance and ambient temperature are both time- and site-specific;
197 results are expected to be sensitive to location, regional weather, and raw water characteristics.

198 The optimization and process model procedures consist of the following steps:

(i) The optimization algorithm arbitrarily initializes a vector of decision variables and passes them to the process model. The decision variables and limits to the values considered in this study are listed in Table 2. The process model then simulates water production over a 24-h, daylong period of operation. Days are subdivided into three periods of variable length: pre-operation (from midnight to the start of the operating period), operation, and post-operation (from the end of the operating period to midnight). During the pre- and post-operation periods, an energy balance based on environmental heat loss is used to calculate the temperature in the hot water tank as a function of time. Through the pre-operation period the system initiates preheating of the makeup water until the start of the operation period. During the period of operation, solar irradiance, solar-thermal and photovoltaic power, temperature in the hot water tank, battery state of charge, and cumulative water purified are calculated at time intervals of 1 min.

(ii) When the 24-hour simulation is complete, the final (midnight) system conditions (e.g., hot water temperature, battery state of charge, and water production) are compared to their initial values. If the conditions are unequal, the initial conditions are reset equal to the calculated final conditions, and the process simulation repeats until the initial and final conditions match, resulting in the simulation of periodic day-to-day operation.

(iii) At this point, the process model calculates the total daily permeate production, and the cost calculation algorithm calculates the capital and recurrent or operational costs of the system using the process model outputs. A financial penalty is assigned to solutions that do not meet the production volume constraint. The penalty is of sufficient magnitude to make such solutions sub-optimal [24, 27].

(iv) The total present value cost of water purification is calculated and annualized. That is, the equipment cost is calculated from the decision variables and economic heuristics and operational costs from operating conditions before all costs are annualized over a 20-year design period using a 5 percent discount operator. Finally, the breakeven price of water is obtained as the total annualized cost divided by the water produced over a one-year period.

(v) The breakeven cost of water is returned to the optimization algorithm. The algorithm adjusts the decision variables, searching for a lower breakeven cost of water, and repeats the process model calculations until that cost can no longer be reduced.

FIGURE 4

TABLE 2

2.3. Cost Calculation.

Cost functions were developed for equipment components including pumps, blowers, vacuum, chiller, hot water tank, condensers, and solar arrays from manufacturers' data (Supplemental material). Off-the-shelf components such as membrane modules and batteries were given a single unit price (manufacturers' data) so that unit cost was independent of scale.

A severe penalty was added to the cost for systems in which the daily water production (calculated from the process simulation) was less than the water production requirement. The application of the penalty is described in detail in our previous studies and it is implemented by applying a coefficient to the cost of water produced ($1,000) [33, 36]. This coefficient is adequately stringent to ensure that solutions that do not meet the water demand requirement are eliminated by the optimization algorithm. It should be noted that while the production goal and actual production is given in m^3 per day of potable water, the penalty is in US dollars.

The objective function represents the amortized cost of water and is set to be minimized during system optimization so that the net present value of the system is equal to zero at the end of the system lifetime. Calculations of membrane and battery replacement, labor, and other operational costs were adapted from Seider et al. [37] and Khayet [11]. The system lifetime was taken as 20 years and the interest rate as 5%. Additional parameters used and assumptions made are detailed in the Supplementary material.

2.4. Process Optimization.

Each MD process was optimized using the particle swarm algorithm in MATLAB following the procedure described in Section 2.2. To investigate the applicability of MD configurations in desalination and treatment of highly saline water, two different feed water salinities were considered: 3.5% and 15%. In all cases, the water production requirement was 10 m^3 d^{-1}. The optimization objective was to find the suite of decision variable values that minimizes total present value costs over a 20-year simulation, thus providing the lowest unit cost of water that results in full cost recovery while satisfying the production requirement (10 m^3 d^{-1}).

The following optimization procedure was used in all cases:

1. *Initialization*: initialize values for each decision variable.

2. *Execution*: run particle swarm process model.
3. *Adjustmen*t: adjust initial values of each decision variable to the optimized values found in Step 2.
4. *Repeat* Steps 2 and 3 until the decision variable values selected by the optimization algorithm equal the input values.

The optimization process was provided with (i) an acceptable range of values for each decision variable (Table 2) to serve as solution boundaries and (ii) initial values for each decision variable within that range.

The particle swarm algorithm logic mimics the social swarming behavior of birds and insects that follow and converge to single pattern or behavior. The algorithm starts by generating an initial set of individuals, each of which is associated with a location, velocity, and an objective function value within the decision variable space. Each individual is ranked based on the proximity to the best value of a neighboring individual. As the algorithm progresses through iterations, individuals move to new positions that are determined based on the best objective function values of neighboring individuals. Repetition of the algorithm results in the particles swarming around an optimal location. Eventually, the algorithm leads all individuals (now a swarm) to a single, location corresponding to the optimal objective function value. At this point, after the procedure yields the same value three times, the algorithm terminates accepting this value as optimal. This protocol increases the odds of the algorithm reaching a global, rather than local, optimum [38-41].

3. Results and discussion

3.1. Optimal Membrane Distillation Systems.

A comparative optimization analysis was performed based on the following design constraints: (i) water production: 10 m^3 d^{-1}; (ii) location: Leupp, Navajo Nation, AZ, USA; (iii) date: March 20; and (iv) NaCl salinity: 3.5 % and 15 %.

March 20 is the spring equinox and represents a median value for both solar irradiance intensity and length of day. Table 3 shows that over a twenty-year lifetime, the optimal VMD system produces water at the lowest cost at \$14.3 m^{-3} compared to the optimal DCMD and SGMD systems. The breakeven costs of water produced by the optimal DCMD and SGMD systems under the same conditions were 47% and 24% higher, respectively (Table 3). Surprisingly, the breakeven

costs for water produced by VMD and SGMD were insensitive to salt concentration in the range 3.5-15 %. However, the same increase in feed water salinity raised the unit cost of water produced by DCMD by about half. At the higher salinity evaluated, the breakeven cost of the DCMD product water was twice that of VMD. VMD and SGMD were also more energetically efficient than DCMD. For the 3.5 % salinity feed solution, the DCMD consumption of energy was more than 50 % higher than the unit energy demand of VMD. At 15 % salinity, the difference was more than 130 %. In both sets of simulations, the energy consumed by SGMD was on the order of 10 % higher than the VMD energy demand (Table 3). Energy demand in both the VMD and SGMD systems was insensitive to salt concentration of the feed solution.

TABLE 3

The primary source of differences in the economic performance and energy efficiencies of the optimized membrane distillation systems was related to thermal energy consumption. The optimization always selected the smallest hot tank volume permitted— for all configurations and both salinities—because thermal energy storage is not economically advantageous in these applications. As expected, thermal collector areas were much larger in DCMD than in other MD configurations. The optimization algorithm selected the highest brine flow rate allowed in each application (Tables 2 and 3), indicating that the optimum value would be still higher. The importance of maintaining temperature in the brine flow throughout the length of the membrane module is evident. The cooling water flow rate is higher for SGMD and VMD systems as there is a higher requirement for heat dissipation from the permeate stream.

For all configurations and salinities, the start and end times of the operational period are approximately the same, with starting time at sunrise and stopping time in late afternoon. This suggests that it is economically and energetically unfavorable to operate on stored thermal or electrical energy. In fact, the battery level of charge was never reduced below 85 %.

3.2. Cost comparison for membrane distillation configurations.

The unit costs of water produced here lie within the range of those previously reported for membrane distillation systems (\$0.40 m^{-3} to \$130 m^{-3}) with cost decreasing as water production objectives increase. All studies reporting a cost less than \$1 m^{-3}, produced water at a rate >75 m^3 d^{-1} [33]. Table 3 and Figures 5-8 support the following observations. Cost contribution of each

major piece of equipment and their relevant costs are shown in Fig. 5. The major components are cost to produce thermal and electrical energy, and cost for the membranes and heat exchangers. The cost to produce thermal energy is equal to that of the thermal collector's area plus the cost of the glycol pump. It is interesting to note that membranes do not comprise a significant portion of the costs. While systems vary in terms of average permeate flux and thus require different membrane areas to meet the water production requirement, the membranes do not account for significant cost differences.

In all systems, thermal energy expenses constitute the most significant portion of the cost. The thermal component is responsible for the high cost of water of the DCMD system, which is less energy efficient than other forms of MD and requires a larger thermal collector area to satisfy thermal energy requirements.

Although the SGMD and VMD systems have similar thermal energy costs, the SGMD system requires a higher condenser area (to condense water from the air stream as opposed to condensing water from a pure water vapor stream in VMD) and more electrical energy to circulate the sweep gas. These two factors are responsible for the modest cost difference between the SGMD and the VMD. Solar thermal collectors make up the largest fraction of cost in all three cases studied (Fig. 5) suggesting that process adjustments that increase efficiency in the generation or use of thermal energy would reduce cost. Results of a previous, related study [33], indicated that membranes were the most significant contributor to total cost. Hollow fiber membranes were selected for use in that study, whereas a flat sheet membrane configuration was chosen here. The two configurations differ substantially in performance and particularly price (\$1,500 m^{-2} for hollow fiber membranes versus \$200 m^{-2} for flat sheet membranes). In this study, the marked reduction in the cost of membranes increased the relative importance of thermal collectors and efficiency in the use of thermal energy. It is possible that with improvements in the efficiency of the current collectors nowadays, the cost of the collectors could be further reduced and thus the membrane component could become an important contributor to the cost again [42]

Feed water salinity had little effect on the cost for the SGMD and VMD systems, but a higher impact on DCMD. As discussed earlier, SGMD and VMD are more thermally efficient than DCMD. As a result, in DCMD salinity changes have a higher impact on the local gradient in water

vapor pressure across the membrane. That, in turn, impacts the amount of heat required to meet the water production target. SGMD and VMD were not affected by changes in salinity.

FIGURE 5

3.3 Analysis of Energy Efficiency.

Figure 6 shows the usable thermal energies that enter the hot water tank from the solar thermal collectors (through the glycol loop), the rejected brine, and the preheated makeup saline feed. Thermal energy exits the hot water tank with the heated saline feed (Stream 3, Figs. 1-3) and through environmental losses (not shown). For SGMD and VMD, heat reentering the hot tank with the rejected brines (Stream 5, Fig. 2 and Stream 4, Fig. 3) is significant compared to the demand for solar-thermal energy. In DCMD, however, the energy returned with rejected brine (Stream 4, Figure 1) is small compared to the input of solar-thermal energy (Stream 1, Fig. 1), especially for the 15% salinity case. Each pass of brine through the module transfers much more heat energy in DCMD than in either SGMD or VMD, increasing the capital investment required for thermal energy collection in DCMD. In no case is the thermal energy in makeup water significant compared to other energy flows. Overall, all three optimized systems have small opportunity for heat recovery. However, if forced to recover more water to increase efficiency, the flow rate of makeup water (equal to water production) may become greater than the flow rate of rejected brine. In high recovery systems, recovery of the heat of vaporization may be more important than in the low recovery systems presented here.

When the salinity of the feed is 15%, more thermal energy is entering from the solar thermal collectors in the DCMD system (in accordance with our previous findings in Section 3.2 where higher cost is allocated to the area of the solar thermal collectors). For SGMD and VMD, less thermal energy in the hot tank is attributed to the rejected brine than for the 3.5% feed salinity. This observation is also expected as more energy is required to meet the production constraint, and thus, we see reduced energy returned to the hot tank. To better understand this finding, if we were to compare the environmental losses for each configuration at 15%, SGMD and VMD have less thermal energy lost to the environment compared to the DCMD, which translates to SGMD and VMD having better use of the thermal energy compared to DCMD.

FIGURE 6

In Fig. 7 we present the energy exiting the membrane modules for each configuration at the two salinities. Notably, for SGMD and VMD systems, most of the thermal energy exits the module with the rejected brine, which is returned to the hot water tank and conserved; the rest of the thermal energy exits the membrane as water vapor. On the other hand, in the DCMD system, most of the thermal energy is used to heat the permeate carrier (distilled water), and less energy remains in the rejected brine to recycle to the hot water tank. This result explains the low thermal efficiency in the DCMD system: heat is lost to the permeate stream due to conduction through the membrane, whereas heat loss through conduction is negligible in the other configurations. Thus, less thermal energy is returned to the hot water tank in DCMD and more energy from thermal collectors is required.

At 15% salinity, DCMD exhibits similar behavior as SGMD and VMD, with most of the thermal energy exiting the module through the rejected brine and a reduction in the amount of thermal energy dissipated by the distilled permeate stream. A possible explanation for this difference with the 3.5% salinity is that the optimization selects a set of decision variables that allows for a higher flowrate of the distillate permeate at the 15% salinity case which in turn translates to lower thermal energy lost to the permeate carrier. In addition, for all three configurations the thermal energy output from the membrane module either with the rejected brine or the permeate is a lower than for the case of the 3.5% salinity. This is a reasonable outcome as more thermal energy is required to meet the constraint of the required amount of water produced.

FIGURE 7

Figure 8 shows the thermal energy exiting the heat exchangers (for DCMD) or condensers (for SGMD and VMD). In the case of DCMD, thermal energy is dissipated by the permeate stream and is eventually discarded by the chiller before returning to the membrane module (Fig. 1). Due to the high thermal conductance through the membrane, the cooling water, reaches higher temperatures, thus more thermal energy is eventually recycled to the hot water tank (Fig. 6). However, as previously discussed, this is still small in comparison to heat from other sources and does not lead to reduced cost (Fig. 5).

In the SGMD and VMD systems, makeup water is preheated by condensing the water vapor exiting the module. In all systems, the thermal energy entering the tank from the preheated makeup water was negligible compared to power inputs from the solar thermal collectors and returning

brine. It is concluded that recycling heat with returned brine is more important than recovery of the heat of vaporization in these simulations. Reasons for this are analyzed below. Note that the optimal cooling water flow rate is larger for SGMD and VMD than for DCMD. This is because the heat recovery device in SGMD and VMD have a dual purpose of condensing water vapor and recover any latent heat from the condensation. To maintain an appreciable temperature difference within the condenser and condense more water, a higher cooling water flow rate is selected by the optimization. Nevertheless, this lowers the temperature of the makeup water, and allows for less energy recovery. If lower flowrates would be selected, higher makeup water temperatures could be achieved, but less permeate would be then condensed. This may require additional membrane modules to reach the water production requirement, which in turn would increase the cost. In DCMD, however, the water production rate is not connected to the cooling water flow rate. Therefore, a lower cooling water flow rate was selected, and larger makeup water temperatures were achievable. The optimized DCMD uses more recovered heat than SGMD (Fig. 8) although this does not lead to an overall cost savings.

FIGURE 8

4. Conclusions and Outlook

Non-steady-state process models were used to simulated solar driven DCMD, SGMD, and VMD. Following optimization steps, the three forms of membrane distillation were compared based on energy and economic efficiencies. Each process was required to produce 10 m^3 d^{-1} of distillate from 3.5% and then 15% (NaCl) salinity water. Optimization was based on total present value cost or energy consumption using the particle swarm algorithm in MATLAB. In all cases, VMD was more cost effective than SGMD or DCMD. At 3.5% initial salinity, the price of water necessary for full recovery of present value costs (20-year design life, r = 0.05 yr^{-1}) was $14.3 per cubic meter. SGMD had a modestly higher electrical energy requirement and higher PV collector area/cost. DCMD proved less energetically efficient, requiring a 50-100 % higher thermal collector area leading to the highest total present value costs. Thermal collectors made up the largest percentage of cost in all cases. Recovery of the heat of vaporization had a much smaller effect on the system energy efficiency than did recycling of rejected brine retained. While this was true for all cases tested, DCMD utilized recovered heat more than SGMD due to the decoupling of the

condensation of water vapor and the preheating of the makeup water. However, this did not provide overall cost savings.

MD is most advantageous when waste thermal energy is used to treat hypersaline waters. However, the membrane configuration plays an important role on the cost of the system which dictates the applicability of the process for desalination. With our current study we showed that an improvement on membrane configuration can reduce the cost of the process by an order of magnitude ($84.7 m^{-3} from previous study to $14.4 m^{-3} current study). Major equipment costs provide information regarding necessary improvements to make this process economically competitive. Further work is required to anticipate cost savings attributable to the use of state-of-the-art solar-thermal collectors in MD systems. Additional work is also required to examine the effect of the design constraints (here chosen arbitrarily) and the impact of geographic and seasonal variables on the cost of water purified by solar MD.

5. Acknowledgments

We acknowledge the Agnese Nelms Haury Program in Environment and Social Justice at the University of Arizona, which supported Dr. Vasiliki Karanikola, and the Campus Executive Laboratory-Driven Research and Development program at Sandia National Laboratories for financial support of Dr. Sarah Moore. We also want to acknowledge the support of Akshay Deshmukh by the NSF Nanosystems Engineering Research Center for Nanotechnology-Enabled Water Treatment (EEC-1449500).

6. References

[1] A.Y. Hoekstra, M.M. Mekonnen, A.K. Chapagain, R.E. Mathews, B.D. Richter, Global Monthly Water Scarcity: Blue Water Footprints versus Blue Water Availability, PLOS ONE, 7 (2012) e32688.
[2] M.M. Mekonnen, A.Y. Hoekstra, Four billion people facing severe water scarcity, Science advances, 2 (2016) e1500323.
[3] M.S. Mauter, I. Zucker, F. Perreault, J.R. Werber, J.-H. Kim, M. Elimelech, The role of nanotechnology in tackling global water challenges, Nature Sustainability, 1 (2018) 166-175.
[4] P.V. Abeygunawardena, Yogesh; Knill, Philipp; Foy, Tim; Harrold, Melissa; Steele, Paul; Tanner, Thomas; Hirsch, Danielle; Oosterman, Maresa; Rooimans, Jaap; Debois, Marc; Lamin, Maria; Liptow, Holger; Mausolf, Elisabeth; Verheyen, Roda; Agrawala, Shardul; Caspary, Georg; Paris, Ramy; Kashyap, Arun; Sharma, Arun; Mathur, Ajay; Sharma, Mahesh; Sperling, Frank;, Poverty and climate change : reducing the vulnerability of the poor through adaptation, in, World Bank, Washington, DC, 2009/01/01, pp. 56.
[5] N.R. Armstrong, R.C. Shallcross, K. Ogden, S. Snyder, A. Achilli, E.L. Armstrong, Challenges and opportunities at the nexus of energy, water, and food: A perspective from the southwest United States, MRS Energy & Sustainability, 5 (2018) E6.
[6] M.A. Shannon, P.W. Bohn, M. Elimelech, J.G. Georgiadis, B.J. Mariñas, A.M. Mayes, Science and technology for water purification in the coming decades, Nature, 452 (2008) 301.
[7] A. Deshmukh, C. Boo, V. Karanikola, S. Lin, A.P. Straub, T. Tong, D.M. Warsinger, M. Elimelech, Membrane distillation at the water-energy nexus: limits, opportunities, and challenges, Energy & Environmental Science, 11 (2018) 1177-1196.
[8] M. Elimelech, W.A. Phillip, The Future of Seawater Desalination: Energy, Technology, and the Environment, Science, 333 (2011) 712.
[9] P.D. Dongare, A. Alabastri, S. Pedersen, K.R. Zodrow, N.J. Hogan, O. Neumann, J. Wu, T. Wang, A. Deshmukh, M. Elimelech, Q. Li, P. Nordlander, N.J. Halas, Nanophotonics-enabled solar membrane distillation for off-grid water purification, Proceedings of the National Academy of Sciences, 114 (2017) 6936.
[10] K.L. Hickenbottom, J. Vanneste, L. Miller-Robbie, A. Deshmukh, M. Elimelech, M.B. Heeley, T.Y. Cath, Techno-economic assessment of a closed-loop osmotic heat engine, Journal of Membrane Science, 535 (2017) 178-187.
[11] M. Khayet, Solar desalination by membrane distillation: Dispersion in energy consumption analysis and water production costs (a review), Desalination, 308 (2013) 89-101.
[12] J. Wu, K.R. Zodrow, P.B. Szemraj, Q. Li, Photothermal nanocomposite membranes for direct solar membrane distillation, Journal of Materials Chemistry A, 5 (2017) 23712-23719.
[13] M.S. El-Bourawi, Z. Ding, R. Ma, M. Khayet, A framework for better understanding membrane distillation separation process, Journal of Membrane Science, 285 (2006) 4-29.
[14] A. Deshmukh, J. Lee, Membrane desalination performance governed by molecular reflection at the liquid-vapor interface, International Journal of Heat and Mass Transfer, 140 (2019) 1006-1022.
[15] V. Karanikola, A.F. Corral, H. Jiang, A. Eduardo Sáez, W.P. Ela, R.G. Arnold, Sweeping gas membrane distillation: Numerical simulation of mass and heat transfer in a hollow fiber membrane module, Journal of Membrane Science, 483 (2015) 15-24.
[16] Z. Wang, T. Horseman, A.P. Straub, N.Y. Yip, D. Li, M. Elimelech, S. Lin, Pathways and challenges for efficient solar-thermal desalination, Science Advances, 5 (2019) eaax0763.

[17] R.D. Gustafson, J.R. Murphy, A. Achilli, A stepwise model of direct contact membrane distillation for application to large-scale systems: Experimental results and model predictions, Desalination, 378 (2016) 14-27.
[18] G.W. Meindersma, C.M. Guijt, A.B. de Haan, Desalination and water recycling by air gap membrane distillation, Desalination, 187 (2006) 291-301.
[19] M. Khayet, M.P. Godino, J.I. Mengual, Theoretical and experimental studies on desalination using the sweeping gas membrane distillation method, Desalination, 157 (2003) 297-305.
[20] S. Lin, N.Y. Yip, M. Elimelech, Direct contact membrane distillation with heat recovery: Thermodynamic insights from module scale modeling, Journal of Membrane Science, 453 (2014) 498-515.
[21] S. Bandini, C. Gostoli, G.C. Sarti, Separation efficiency in vacuum membrane distillation, Journal of Membrane Science, 73 (1992) 217-229.
[22] E.K. Summers, H.A. Arafat, J.H. Lienhard, Energy efficiency comparison of single-stage membrane distillation (MD) desalination cycles in different configurations, Desalination, 290 (2012) 54-66.
[23] L. Eykens, T. Reyns, K. De Sitter, C. Dotremont, L. Pinoy, B. Van der Bruggen, How to select a membrane distillation configuration? Process conditions and membrane influence unraveled, Desalination, 399 (2016) 105-115.
[24] S. Al-Obaidani, E. Curcio, F. Macedonio, G. Di Profio, H. Al-Hinai, E. Drioli, Potential of membrane distillation in seawater desalination: Thermal efficiency, sensitivity study and cost estimation, Journal of Membrane Science, 323 (2008) 85-98.
[25] F. Banat, N. Jwaied, Economic evaluation of desalination by small-scale autonomous solar-powered membrane distillation units, Desalination, 220 (2008) 566-573.
[26] V.A. Bui, L.T.T. Vu, M.H. Nguyen, Simulation and optimisation of direct contact membrane distillation for energy efficiency, Desalination, 259 (2010) 29-37.
[27] H. Chang, C.-L. Chang, C.-Y. Hung, T.-W. Cheng, C.-D. Ho, Optimization study of small-scale solar membrane distillation desalination systems (s-SMDDS), International journal of environmental research and public health, 11 (2014) 12064-12087.
[28] H.M. Laborde, K.B. França, H. Neff, A.M.N. Lima, Optimization strategy for a small-scale reverse osmosis water desalination system based on solar energy, Desalination, 133 (2001) 1-12.
[29] R.B. Saffarini, E.K. Summers, H.A. Arafat, J.H. Lienhard V, Economic evaluation of stand-alone solar powered membrane distillation systems, Desalination, 299 (2012) 55-62.
[30] G. Zaragoza, J.A. Andrés-Mañas, A. Ruiz-Aguirre, Commercial scale membrane distillation for solar desalination, npj Clean Water, 1 (2018) 20.
[31] G. Zuo, G. Guan, R. Wang, Numerical modeling and optimization of vacuum membrane distillation module for low-cost water production, Desalination, 339 (2014) 1-9.
[32] G. Zuo, R. Wang, R. Field, A.G. Fane, Energy efficiency evaluation and economic analyses of direct contact membrane distillation system using Aspen Plus, Desalination, 283 (2011) 237-244.
[33] S.E. Moore, S.D. Mirchandani, V. Karanikola, T.M. Nenoff, R.G. Arnold, A. Eduardo Sáez, Process modeling for economic optimization of a solar driven sweeping gas membrane distillation desalination system, Desalination, 437 (2018) 108-120.
[34] V. Karanikola, A.F. Corral, H. Jiang, A.E. Sáez, W.P. Ela, R.G. Arnold, Effects of membrane structure and operational variables on membrane distillation performance, Journal of Membrane Science, 524 (2017) 87-96.

[35] A. Deshmukh, M. Elimelech, Understanding the impact of membrane properties and transport phenomena on the energetic performance of membrane distillation desalination, Journal of Membrane Science, 539 (2017) 458-474.
[36] A. Homaifar, C.X. Qi, S.H. Lai, Constrained Optimization Via Genetic Algorithms, SIMULATION, 62 (1994) 242-253.
[37] D.R.L. W. D. Seider, J. D. Seader, S. Widagdo, R. Gani, K. M. Ng, Product and Process Design Principles: Synthesis, Analysis, and Evaluation, 4th ed., John Wiley & Sons Inc., New York, 2009.
[38] MathWorks, Particle Swarm Options, in, 2017.
[39] J. Kennedy, R. Eberhart, Particle swarm optimization, in: Proceedings of ICNN'95 - International Conference on Neural Networks, 1995, pp. 1942-1948 vol.1944.
[40] Eberhart, S. Yuhui, Particle swarm optimization: developments, applications and resources, in: Proceedings of the 2001 Congress on Evolutionary Computation (IEEE Cat. No.01TH8546), 2001, pp. 81-86 vol. 81.
[41] A. Khare, S. Rangnekar, A review of particle swarm optimization and its applications in Solar Photovoltaic system, Applied Soft Computing, 13 (2013) 2997-3006.
[42] A.B. Pouyfaucon, L. García-Rodríguez, Solar thermal-powered desalination: A viable solution for a potential market, Desalination, 435 (2018) 60-69.
[43] M. Khayet, T. Matsuura, Membrane Distillation: Principles and applications, Elsevier, Oxford, 2011.

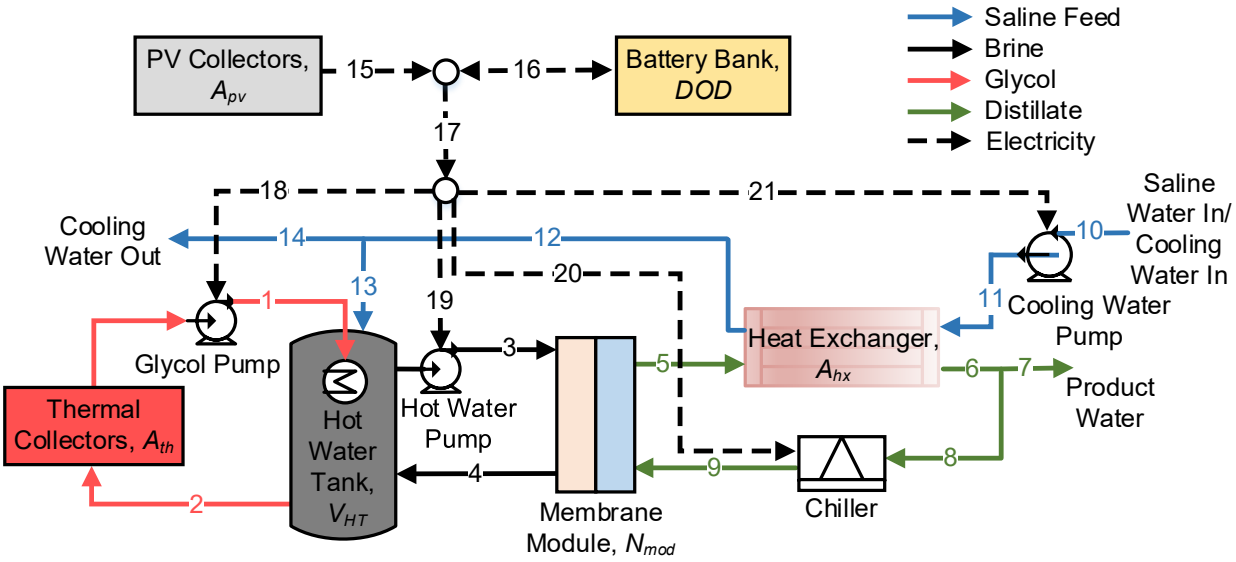

Fig. 1. Flow diagram of solar powered direct contact membrane distillation (DCMD) process. See text.

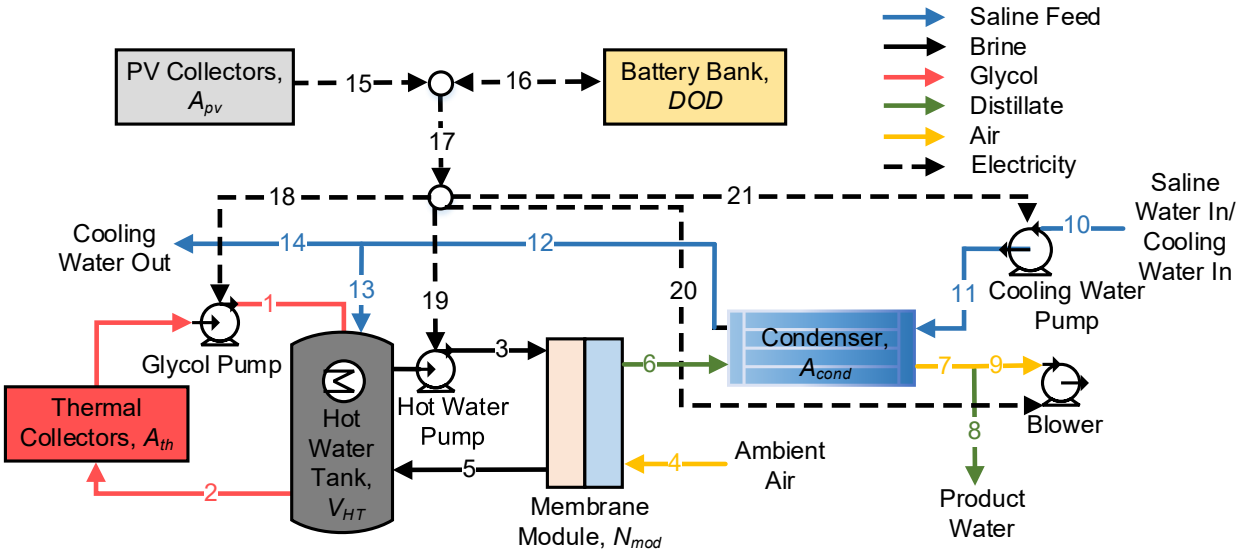

Fig. 2. Flow diagram of solar powered sweeping gas membrane distillation (SGMD) process. See text.

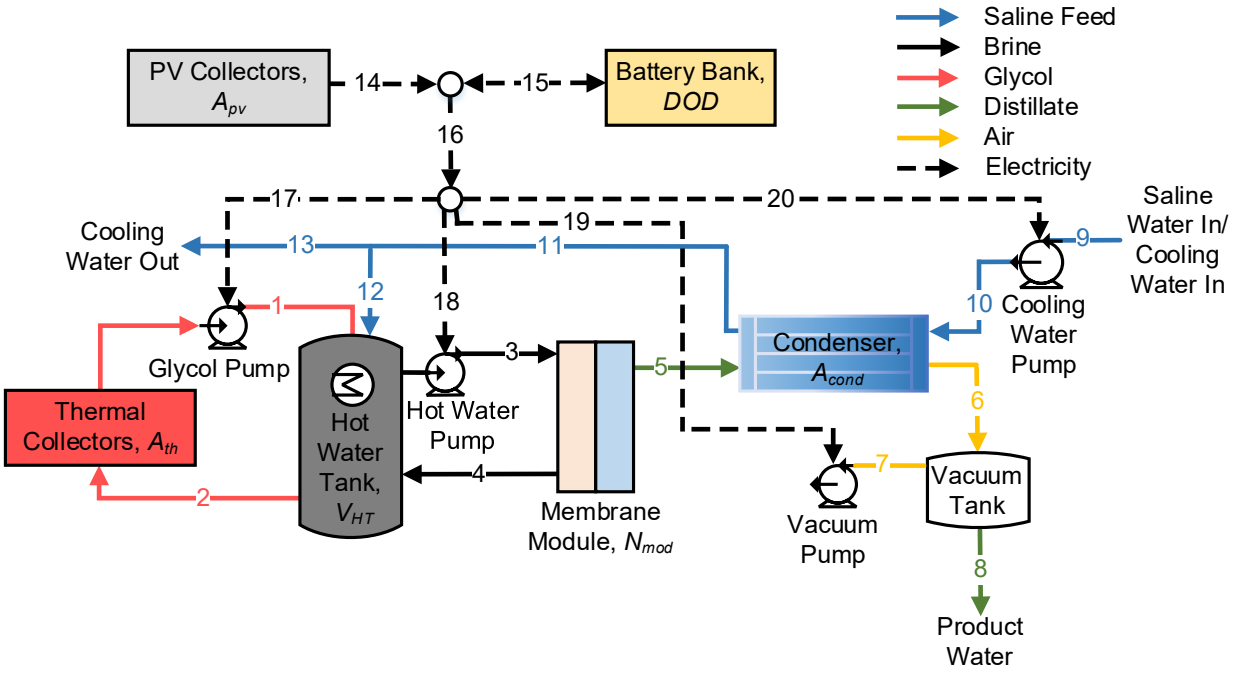

Fig. 3. Flow diagram for solar powered vacuum membrane distillation (VMD) process. See text.

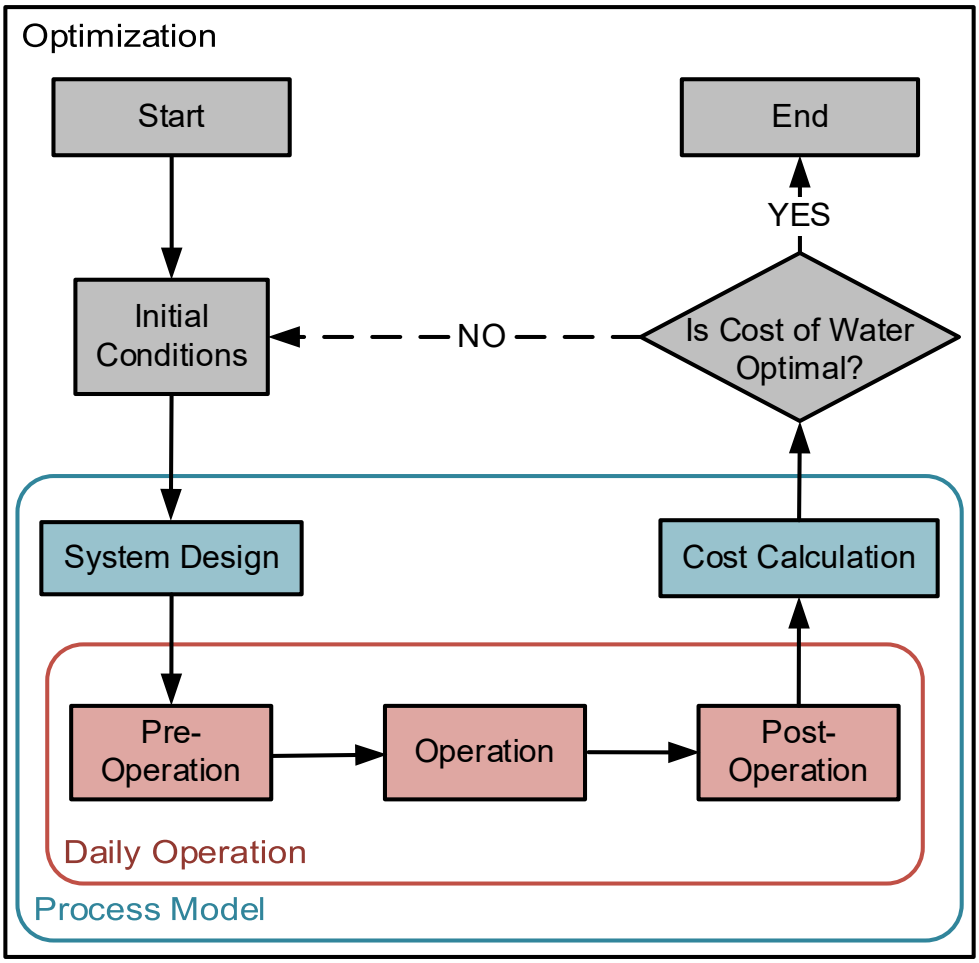

Fig. 4. Overview of process modeling and optimization. The optimization selects decision variable values and passes them to the process model, which calculates the cost of water as a function of the decision variables. The first step of the modeling loop is the decision variable initialization, followed by the process model and the system design, and finally the simulation of daily operation. the daily operation is broken down into three sections: pre-operation (from midnight to the start of the operating period), operation, and post-operation (from the end of the operating period to midnight). Between the water production start and end time, the simulation also calculates the water produced, which varies between configurations. After daily operation is simulated, the final values of the decision variable are compared to their initial values. If they are not equal, the initial conditions are set equal to their final conditions. The process simulation repeats until the initial and final conditions match, resulting in a simulation of day-to-day operation rather than start-up. Finally, the cost of water is calculated. This value is returned to the optimization algorithm. The algorithm repeats multiple times until the values of the objective function swarming around a single optimal location. The algorithm terminates after it produced the same optimal value three times. If the cost is non-optimal, the algorithm selects new decision variable values and repeats the process model until the cost of water is minimized.

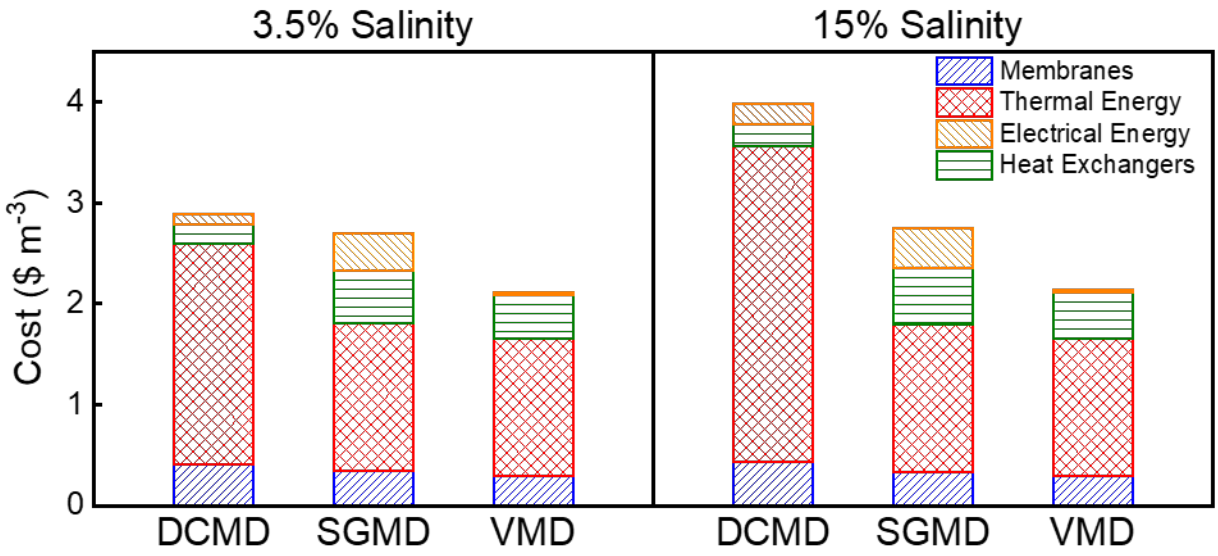

Fig. 5. Selected cost components for optimal DCMD, SGMD, and VMD systems. Note that membrane costs are due to membrane capital and replacement costs; electrical costs include the capital costs of photovoltaic panels and batteries and replacement costs of batteries. Several significant portions of the cost of water are excluded to emphasize the importance of key pieces of equipment. Excluded costs include piping, equipment such as pumps, chillers, and tanks, miscellaneous capital expenses, labor and maintenance expenses, and interest fees.

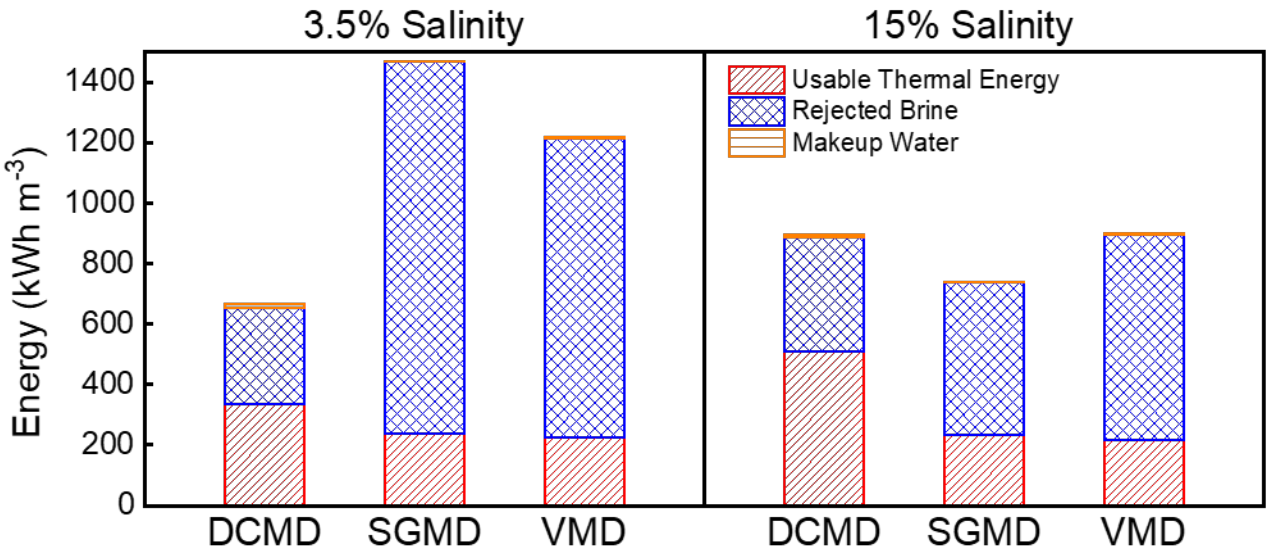

Fig. 6. Thermal energy from various sources entering the hot water tank integrated over time throughout one day of operation in the optimal DCMD, SGMD, and VMD systems. In all three configurations, energy for distillation is provided by the solar-thermal collectors, from rejected brine returned to the tank from the membrane modules, and as makeup water pre-heated using the heat of condensation of permeate (in the heat exchanger in DCMD and the condenser in SGMD and VMD).

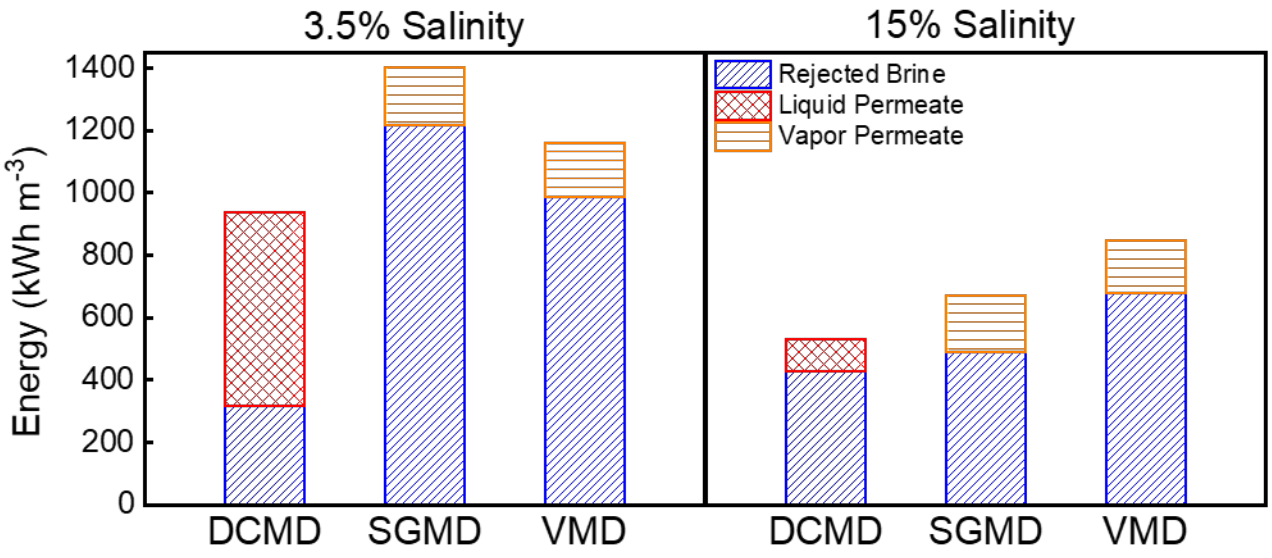

Fig. 7. Thermal energy exiting the membrane modules over one day of operation in the optimal DCMD, SGMD, and VMD systems. In all three configurations, thermal energy is supplied to the modules in the hot brine (Stream 3, Figures 1-3). Thermal energy is lost from the modules in the rejected brine (all systems), the cold contact fluid ((Stream 5, Fig. 1, DCMD) or water vapor (SGMD, Stream 6 and VMD, Stream 5).

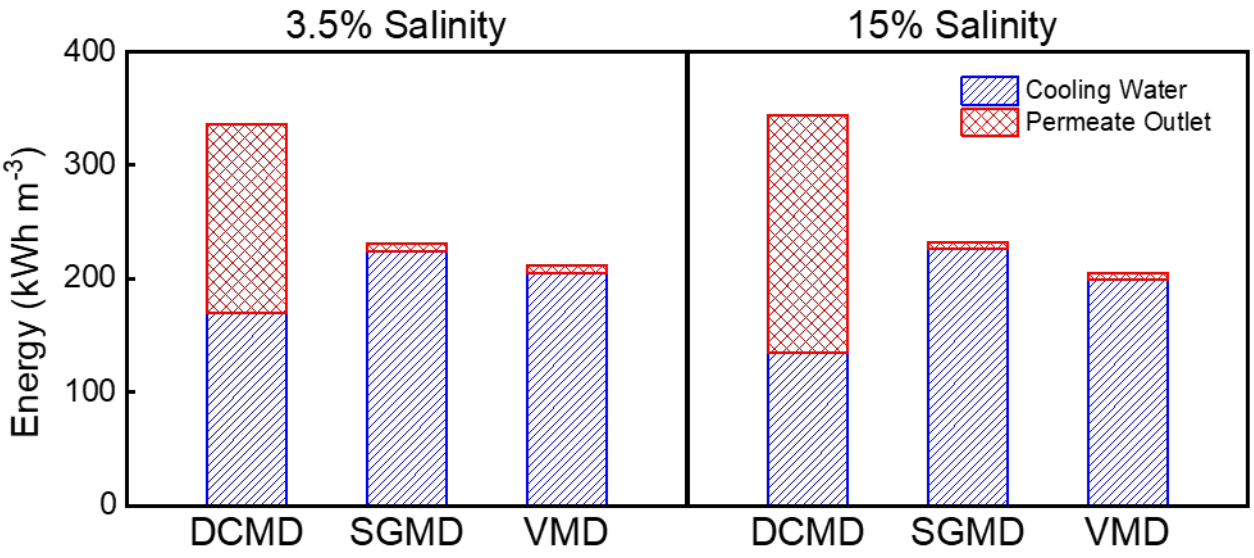

Fig. 8. Thermal energy distribution from the heat exchangers (DCMD) or condensers (SGMD and VMD) integrated over time throughout one day of operation in the optimal DCMD, SGMD, and VMD systems. In the SGMD and VMD systems, nearly all entering energy exits in the cooling water, where a portion of that stream may be fed to the hot water tank to recycle the heat of vaporization of water.

Table 1. Qualitative comparison between membrane distillation configurations across a wide variety of MD performance metrics. [13, 15, 17, 18, 20, 22-25, 32, 43]

Metric	DCMD	SGMD	VMD	AGMD
Conceptual Simplicity	★★★	★☆☆	★☆☆	★★☆
Thermal Efficiency	★☆☆	★★☆	★★★	★☆☆
Mass Transfer Efficiency	★☆☆	★★★	★★★	★☆☆
Heat Recovery	★★★	★☆☆	★☆☆	★★★
Resistance to Wetting	★★☆	★★★	★☆☆	★★★

Table 2. Decision variables and the upper and lower bounds of value selection available to the optimization algorithm.

Decision Variables	Upper and Lower Bounds
Membrane Area (m^2)	1 – 100
Hot Water Tank Volume (L)	100 – 2000
PV Collector Area (m^2)	1 – 100
Thermal Collector Area (m^2)	1 – 5000
Brine Flow Rate (L min^{-1})	1 – 5
Distillate Flowrate (L min^{-1})	0.1 – 50
Air Flow Rate (L min^{-1})	0.02 – 200
Vacuum Pressure (kPa)	10 – 90
Cooling Water Flow Rate (L min^{-1})	1 – 20
Heat Exchanger Area (m^2)	0.01 – 2
Depth of Discharge	0.01 – 1
Start Time	00:00 (Midnight) – 12:00 (Noon)
End Time	12:00 (Noon) – 00:00 (Midnight)
Water Production Start Time	00:00 (Midnight) – 12:00 (Noon)
Water Production End Time	12:00 (Noon) – 00:00 (Midnight)

Table 3. Decision variable values leading to minimal cost for three different solar MD configurations treating water of two salinities and system performance indicators, including cost of water and specific energy consumption (SEC).

Feed Salinity	3.5 %			15 %		
MD Configuration	DCMD	SGMD	VMD	DCMD	SGMD	VMD
Cost of Water ($\$ m^{-3}$)	21.0	17.7	14.3	29.7	18.6	14.4
Specific Energy Consumption ($kWh\ m^{-3}$)	1017	729	650	1536	719	660
Membrane Area (m^2)	39	33	28	42	32	28
Hot Water Tank Volume (L)	100	100	100	100	100	100
PV Collector Area (m^2)	12	50	4	29	51	4
Thermal Collector Area (m^2)	1050	700	650	1500	700	650
Brine Flow Rate ($L\ min^{-1}$)	5	5	5	5	5	5
Distillate Flowrate ($L\ min^{-1}$)	2.5	N/A	N/A	5	N/A	N/A
Air Flow Rate ($L\ min^{-1}$)	N/A	180	N/A	N/A	180	N/A
Vacuum Pressure (kPa)	N/A	N/A	90	N/A	N/A	90
Cooling Water Flow Rate ($L\ min^{-1}$)	2	14	10	2	12	8
Heat Exchanger Area (m^2)	0.05	0.80	0.40	0.05	1.00	0.45
Depth of Discharge	0.90	1.00	0.85	0.9	0.95	0.85
Start Time	5:00	5:00	6:00	5:00	5:20	6:00
End Time	15:30	15:40	15:50	17:30	15:40	16:40
Water Production Start Time	06:00	06:10	06:00	06:00	06:00	06:00
Water Production End Time	15:30	15:40	15:50	16:20	15:30	16:40